Yang, L., Martínez Piqueras, G., Muñoz Ferreras, J.M. & Gómez García, R. 2022, "Planar high-order broad-band bandpass filters based on two-stage quadrature couplers and their digital modeling", in 2022 24th International Microwave and Radar Conference (MIKON), Gdansk, Poland, 2022, pp. 1-5.

Available at http://dx.doi.org/10.23919/MIKON54314.2022.9924820

Planar High-Order Broad-Band Bandpass Filters Based on Two-Stage Quadrature Couplers and Their Digital Modeling

Li Yang[#1], Gaspar Martínez-Piqueras[#2], José-María Muñoz-Ferreras[#3], Roberto Gómez-García[#4]

[#]Dept. Signal Theory and Commun., University of Alcalá, Alcalá de Henares, Madrid, Spain
[1]li.yang@uah.es, [2]gasparpique@gmail.com, [3]jm.munoz@uah.es, [4]roberto.gomez.garcia@ieee.org

***Abstract* — Planar two-stage branch-line directional power couplers are applied in this paper to the design of transversal-signal-interference high-order wide-band bandpass filters (BPFs) with very-sharp-rejection characteristics. In comparison with the previously-reported experimental BPF demonstrators of their precursors—i.e., those using transversal filtering sections (TFSs) with one-stage branch-line couplers loaded by longer dissimilar stubs—, an enlarged-bandwidth passband with a higher number of in-band reflection zeros and lower amplitude variation can be obtained. Moreover, multiple transmission zeros (TZs) can be created in the out-of-band region owing to the intrinsic signal-energy cancelation phenomena of the transversal signal-interference philosophy, which result in high-selectivity filtering capabilities. As further conceptual understanding of the devised two-stage-coupler signal-interference BPFs, a digital-modeling interpretation for various illustrative synthesis examples is provided. In addition, for experimental-validation purposes, single- and two-TFS-based microstrip prototypes of wide-band BPFs centered at 2 GHz are manufactured and characterized. In these circuits, inter-digital-type input/output feeding sections are co-integrated. They allow to extend the lower/upper stopband bandwidths with regard to those inherent to their isolated two-stage-coupler-based TFSs.**

***Keywords* — Bandpass filter (BPF), branch-line coupler, transmission zero (TZ), transversal filtering section (TFS), two-stage coupler, wide-band coupler, wide-band filter.**

I. Introduction

Quadrature directional power couplers are fundamental RF-signal-distribution components in a large variety of microwave subsystems. For example, they are widely employed in reflective-type phase shifters, mixers, I/Q and QPSK modulators, Doherty power amplifiers, or crossovers in planar Butler matrices for array antennas [1]–[5]. They have also been exploited as basic building blocks in different microwave filter applications, either to directly shape the filtering functionality in unconventional filter circuit networks—e.g., the so-called "signal-interference transversal filtering sections (TFSs)" extrapolated from transversal digital filter concepts to the RF domain [6]–[8]—or to incorporate some other relevant operational features in the overall filtering device—e.g., symmetrical RF-power-reflectionless capability in two-branch absorptive filter architectures [9], [10].

In the particular case of branch-line-coupler-based TFSs, they have been used to realize single- and dual-band bandpass filters (BPFs) with sharp-rejection properties [6], [7]. Other types of power-distribution circuits have also been employed under the signal-interference philosophy to microwave filter design [11]–[13]. To this aim, the directional coupler is loaded with different-length stubs in its direct and coupled ports. In this manner, a filtering network with two electrical paths is configured when the isolated port of the coupler is taken as the overall output terminal. By means of constructive and destructive signal-energy interactions among these two electrical paths that allow to shape the passband and stopband regions, respectively, very-abrupt cut-off slopes can be attained through transmission-zero (TZ) creation. Nevertheless, due to both the specific frequency-dependent behavior of the basic branch-line coupler and the lengths of the added stubs, a relatively-rounded passband with moderate bandwidth was obtained in the associated demonstrative BPF prototypes reported in [6]. Although such bandwidth may be broadened by using shorter stubs after a proper adjustment, this is attained for a limited number of in-band reflection zeros in the single TFS. Besides, the spectral periodicity inherent to the basic TFS leads to narrow-band stopbands in its bandpass transfer function as a major drawback for their applicability.

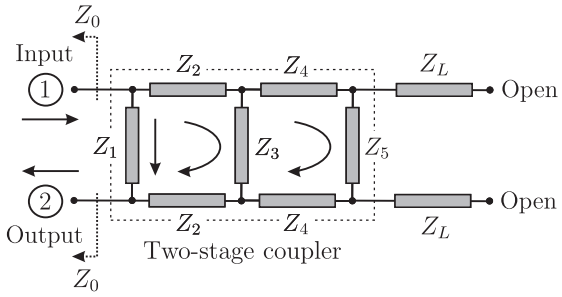

Fig. 1. Circuit detail of the proposed two-stage-branch-line-coupler-based bandpass TFS with three electrical paths (Z_1, Z_2, Z_3, Z_4, Z_5, and Z_L: characteristic impedances; Z_0: reference impedance; the electrical lengths of all transmission-line segments are equal to 90° at the design frequency f_d).

In this paper, bandpass TFSs based on two-stage branch-line couplers loaded by shorter equal-length stubs are proposed to overcome the aforementioned limitations. It is demonstrated that sharp-rejection high-order wide-band BPF circuits with an increased number of in-band reflection zeros and a reduced in-band amplitude variation can be designed with them. Furthermore, inter-digital-type input/output feeding sections can be incorporated in these BPFs to increase the rejection levels and spectral width of their stopbands. A digital-modeling framework for the engineered two-stage-branch-line-coupler-based signal-interference BPFs, which allows a complementary interpretation of their zero/pole characteristics from a discrete-time perspective towards a better understanding, is also provided. Besides, for experimental-demonstration purposes, simulation and measurement results of 2-GHz microstrip prototypes consisting of single- and two-TFS BPFs are also shown.

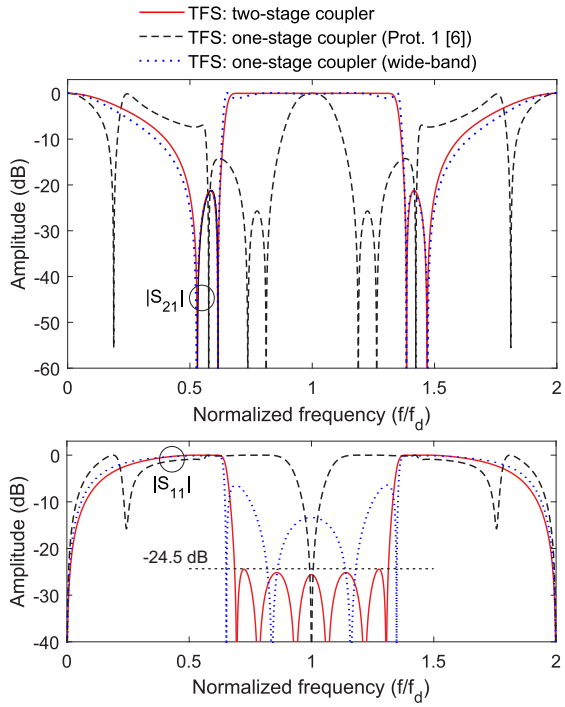

Fig. 2. Theoretical power transmission ($|S_{21}|$) and reflection ($|S_{11}|$) responses of design examples corresponding to (i) the two-stage-coupler-based TFS in Fig. 1 ($Z_1 = 1.966Z_0$, $Z_2 = 0.91Z_0$, $Z_3 = 1.294Z_0$, $Z_4 = 1.004Z_0$, $Z_5 = 2.388Z_0$, and $Z_L = 2.486Z_0$), (ii) the basic one-stage-coupler-based TFS associated to the first prototype of [6] (Fig. 1 of [6]: $Z_1 = 0.62Z_0$, $Z_2 = Z_{L1} = Z_{L2} = Z_0$, $\theta_1(f_d) = 90^o$, and $\theta_2(f_d) = 450^o$), and (iii) a wider-band TFS version of (ii) for the same out-of-band TZ positioning as in (i) (Fig. 1 of [6]: $Z_1 = 0.87Z_0$, $Z_2 = 0.8Z_0$, $Z_{L1} = Z_{L2} = 0.66Z_0$, and $\theta_1(f_d) = \theta_2(f_d) = 90^o$).

II. Theoretical Foundations

A. Operational Principle and Synthesis Examples

The circuit detail of the proposed two-stage-branch-line-coupler-based bandpass TFS is presented in Fig. 1. Like its TFS precursor made up of a basic one-stage coupler that was reported in [6], open-ended stubs are loaded at its direct and coupled ports. Hence, a bandpass filtering action is obtained in the resulting multi-electrical-path circuit network through constructive/destructive transversal-signal-interference effects. The in-band and out-of-band characteristics of such filtering response arw determined by both the spectral behavior of its constituent coupler and its loading stubs. Hence, it is expected that an optimized performance can be attained in this new TFS approach in Fig. 1 when compared to its preliminary version in [6], since a different directional power coupler—i.e., two-stage versus one-stage, hence exhibiting more design variables as degrees of freedom—is employed. Furthermore, identical shorter-length loading stubs can be adopted instead of dissimilar ones in the case that a broader-band bandpass filtering action is targeted.

For illustration purposes, the theoretical power transmission and reflection responses for a quasi-equiripple-type design example of the two-stage-branch-line-coupler-based bandpass TFS in Fig. 1 and the basic one—which corresponds to the first practical prototype that was developed in [6]—are plotted in Fig. 2. As previously outlined, due to the large number of design parameters involved in this two-stage-coupler TFS, an optimization procedure was applied

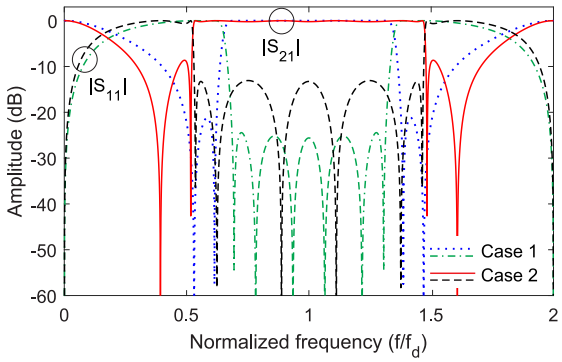

Fig. 3. Bandwidth control in terms of theoretical power transmission ($|S_{21}|$) and reflection ($|S_{11}|$) responses of the two-stage-coupler-based TFS in Fig. 1 (case 1: $Z_1 = 1.966Z_0$, $Z_2 = 0.91Z_0$, $Z_3 = 1.294Z_0$, $Z_4 = 1.004Z_0$, $Z_5 = 2.388Z_0$, and $Z_L = 2.486Z_0$; case 2: $Z_1 = 1.746Z_0$, $Z_2 = 0.81Z_0$, $Z_3 = 1.194Z_0$, $Z_4 = 1.084Z_0$, $Z_5 = 2.388Z_0$, and $Z_L = 0.846Z_0$).

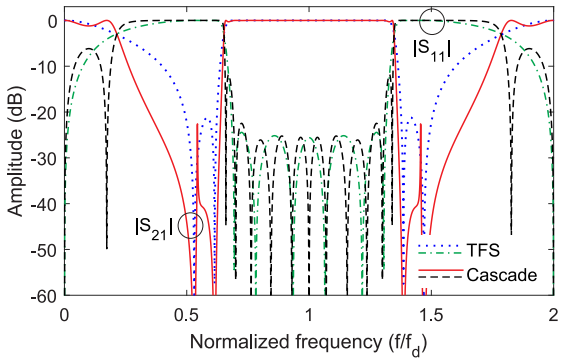

Fig. 4. Theoretical power transmission ($|S_{21}|$) and reflection ($|S_{11}|$) responses of a design example of two-TFS-based BPF and its constituent TFS ($Z_1 = 1.966Z_0$, $Z_2 = 0.91Z_0$, $Z_3 = 1.294Z_0$, $Z_4 = 1.004Z_0$, $Z_5 = 2.388Z_0$, and $Z_L = 2.486Z_0$; inter-TFS cascading line: electrical length at f_d of 180^o and characteristic impedance of $1.06Z_0$).

for this design example. As can be seen, an improved transfer function in terms of bandwidth and increased number of in-band reflection zeros is obtained, making it suitable for broad-band filtering applications. Note that such bandwidth-broadening feature can be equally attained in the one-stage-coupler TFS by also using identical shorter-length stubs. However, an increased amount of in-band reflection zeros—six versus four—and higher in-band power-matching levels—which lead to a reduced in-band amplitude variation—are attained in the two-stage-coupler TFS. This is proven in Fig. 2 through comparison with a reference design of wide-band bandpass TFS using the one-stage coupler and adjusted to exhibit the same stopband-TZ locations.

Finally, the versatility of the devised two-stage-branch-line-coupler-based bandpass TFS for flexible bandwidth adjustment and higher-order BPF designs based on in-series-cascaded TFS replicas is verified in Figs. 3 and 4, respectively. In particular:

- By decreasing the value of the characteristic impedance of the loading open-ended stubs, broader passband widths can be realized. This is corroborated in Fig. 3, which also reveals how such bandwidth enlargement is attained at the expense of lower in-band power-matching levels and reduced out-of-band power-attenuation levels in the stopband lobe as the

Table 1. Coefficients a_k and b_k of the digital model associated to the power transmission response of the single TFS in Fig. 4.

Coefficient Values					
k	a_k	b_k	k	a_k	b_k
0	1.0000	0.2992	5	−0.5570	−0.6008
1	1.2248	0.6270	6	0.0140	−0.6270
2	0.3993	0.6008	7	0.1324	−0.2992
3	−0.9416	0.4143	8	0.0543	–
4	−1.3261	−0.4143	9	–	–

Table 2. Coefficients a_k and b_k of the digital model associated to the power transmission response of the two-TFS-based BPF in Fig. 4.

Coefficient Values					
k	a_k	b_k	k	a_k	b_k
0	1.0000	0.0883	10	−3.7604	0.6235
1	2.4689	0.3699	11	−2.4986	0.9870
2	2.2728	0.7419	12	0.9245	0.7419
3	−1.2368	0.9870	13	2.3663	0.3699
4	−5.5342	0.6235	14	1.2536	0.0883
5	−5.4693	−0.3758	15	−0.1876	–
6	−0.2114	−1.4340	16	−0.5678	–
7	5.0401	−2.0015	17	−0.2882	–
8	4.7165	−1.4340	18	−0.0543	–
9	−0.2341	−0.3758	19	–	–

main design trade-offs.

- Higher stopband attenuation levels and more-abrupt cut-off slopes can be achieved in a two-TFS-cascaded BPF design when compared to its building TFS. Whereas the number of in-band reflection zeros is increased from six to eleven as attested by Fig. 4, the appearance of some narrow-band spikes in the out-of-band region that are intrinsic to the inter-TFS in-series-cascade process—as it was carefully studied in [14]—is also observed.

B. Digital-Modeling Interpretation

The proposed TFS topology in Fig. 1 and higher-order BPF designs based on cascaded replicas are shaped by the interconnection of commensurate transmission-line segments, which confer upon them the frequency-periodicity feature [15], [16]. This means that the power transmission response $|S_{21}|$ of the ideal lossless designs of the one-stage-coupler-based TFS and the two-TFS-based BPF in Fig. 4 is spectrally periodic of period $2f_d$. As a consequence, the real-valued coefficients a_k, $k = 0, 1, \ldots, N$, and b_k, $k = 0, 1, \ldots, M$, of the transfer function of the discrete-time linear time-invariant system associated to each transmission scattering parameter can be extracted, after the application of the theoretical procedure detailed in [15], [16].

The referred coefficients a_k and b_k corresponding to the ideal design of the TFS in Fig. 4 are detailed in Table 1. As can be seen, the orders of the polynomials of the transfer function are $M = 7$ and $N = 8$. On the other hand, the coefficients a_k and b_k associated to the ideal design of the two-TFS-based BPF in Fig. 4 are listed in Table 2. Note that the polynomial orders are increased to $M = 14$ and $N = 18$, thus confirming the enhanced selectivity for the cascade design when compared to that of the single TFS.

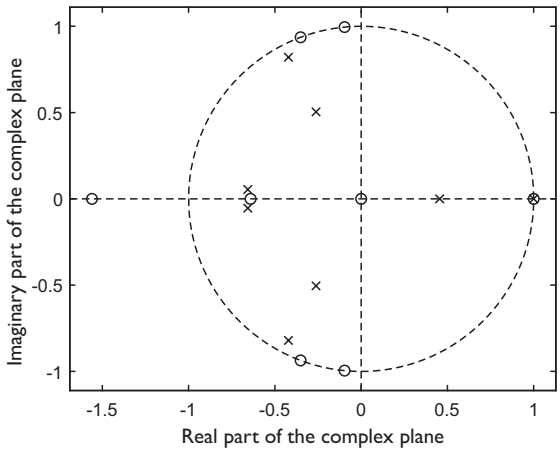

Fig. 5. Zero-pole diagram of the digital system associated to the transmission scattering parameter of the single TFS in Fig. 4 (poles are represented with symbol "x"; zeros are represented with symbol "o"; numbers indicate the multiplicity of the root).

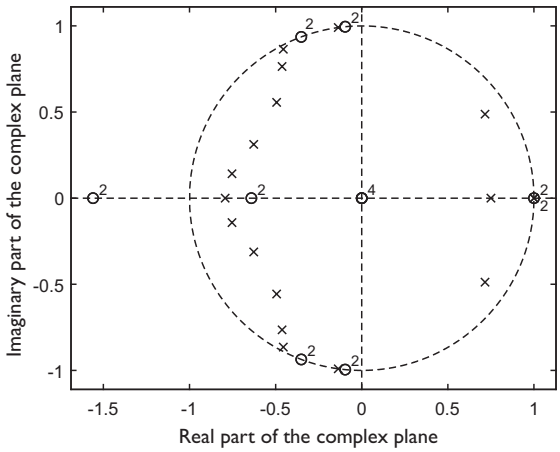

Fig. 6. Zero-pole diagram of the digital system associated to the transmission scattering parameter of the two-TFS-based BPF in Fig. 4 (poles are represented with symbol "x"; zeros are represented with symbol "o"; numbers indicate the multiplicity of the root).

The zero-pole diagrams associated to the transmission scattering parameters of the single TFS and the two-TFS-based BPF in Fig. 4 are depicted in Figs. 5 and 6, respectively. As can be seen, the poles appear contained within the unit circumference, which agrees with the passivity property of the referred microwave circuits. Moreover, the transmission zeros are correctly located on the unit circumference and the poles situated in the left-hand side of the complex plane correspond to the in-band reflection zeros observed in Fig. 4, which are increased in number from six to eleven. Finally, the quasi zero-pole cancelations observed in Fig. 6 near the imaginary axis permit to explain the narrow-band spikes occurring for the cascade design.

III. Experimental Results

To verify the practical viability of the proposed two-stage-quadrature-coupler-based TFS for the design of sharp-rejection high-order broad-band BPFs, two microstrip prototypes with 2-GHz center frequency have been fabricated and measured. They correspond to a broad-band TFS with 3-dB fractional bandwidth equal to 70% and a two-stage BPF composed of the in-series cascade connection of two

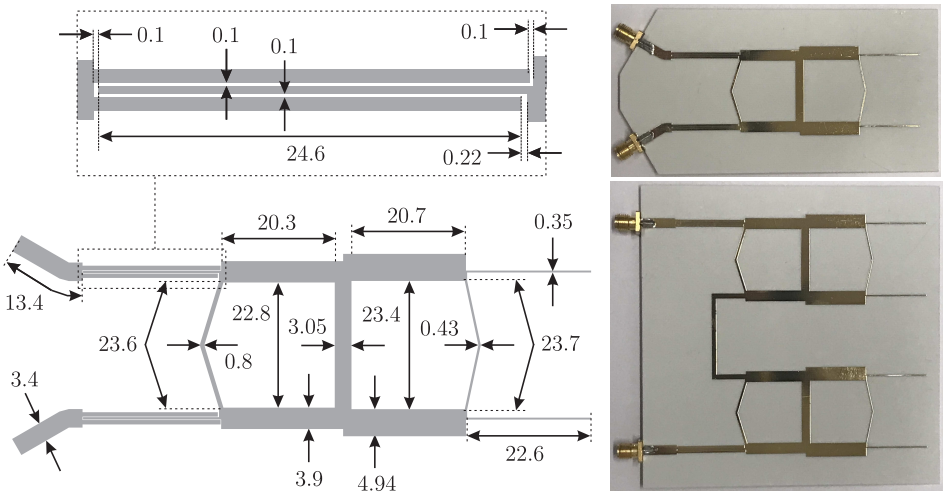

Fig. 7. Photographs of the manufactured microstrip prototypes of of wide-band BPFs: single-TFS (including layout with dimensions in mm) and two-TFS-based circuits.

replicas of this TFS. The theoretical design of the TFS was carried out by applying the design guidelines previously expounded in order to meet the intended passband-width requisite while assuring high in-band power-matching levels. For prototype fabrication, a Rogers 4003C microstrip substrate with the following parameters was employed: relative dielectric permittivity $\varepsilon_r = 3.38$, dielectric thickness $H = 1.524$ mm, metal thickness $t = 35$ μm, and dielectric loss tangent $\tan(\delta_D) = 0.0027$. The photographs of the constructed microstrip BPF prototypes are provided in Fig. 7. The layout with dimensions of the single-TFS circuit is also provided for the sake of reproducibility. As shown, in order to further increase the lower/upper stopband bandwidths and power-attenuation levels with regard to those offered by the TFS—as a limitation also shared by other prior-art TFSs without coupled-line stages—, input/output inter-digital-type feeding sections as in [17] and [18] were inserted in these wide-band BPF circuits. This is illustrated in Fig. 8, which compares the electromagnetically-(EM)-simulated (with Ansys HFSS) power transmission and reflection responses of the designed TFS with inter-digital-type input/output feeding sections (Fig. 7) and the theoretical ones of the ideal TFS (Figs. 1 and 2 for $f_d = 2$ GHz and $Z_0 = 50$ Ω) without such feeding stages, thus proving the referred out-of-band response enhancement.

The EM-simulated and measured (with a Keysight 5224A network analyzer) power-transmission and reflection responses of the two manufactured microstrip prototypes are depicted in Fig. 9, which are in fairly-close agreement. Note that the out-of-band spikes inherent to the inter-TFS cascading process become largely attenuated in the two-TFS BPF circuit thanks to the action of the inter-digital-type input/output feeding stages. However, this is achieved at the expense of some in-band insertion-loss increase. The main measured performance metrics of the developed BPF prototypes are detailed below:

- Single TFS: center frequency of 1.98 GHz, 3-dB absolute bandwidth of 1.44 GHz (i.e., 72.7% in relative terms), minimum in-band power-insertion-loss level equal to 0.8 dB, minimum in-band power-matching level of 16.7 dB, and rejection rates for the lower and upper cut-off slopes—measured from the corresponding 3-dB cut-off frequency to the closest-TZ frequency—of 150 dB/GHz and 215 dB/GHz, respectively.
- Two-TFS BPF: center frequency equal to 1.97 GHz, 3-dB absolute bandwidth of 1.385 GHz (i.e., 70.2% in relative terms), minimum in-band power-insertion-loss level of 1.4 dB, minimum in-band power-matching level of 14.3 dB, and rejection rates for the lower and upper passband-to-stopband transitions of 405 dB/GHz and 218 dB/GHz, respectively.

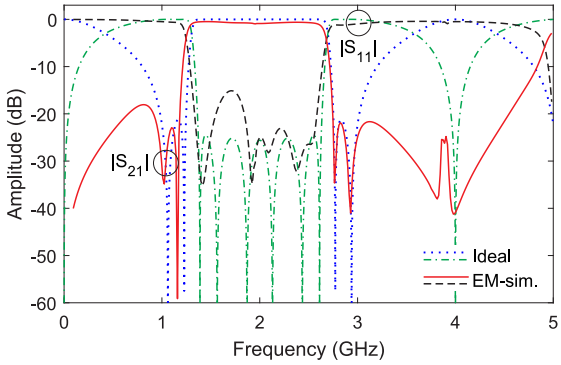

Fig. 8. Theoretical and EM-simulated power transmission ($|S_{21}|$) and reflection ($|S_{11}|$) responses of the designed microstrip TFS (i.e., layout in Fig. 7 with inter-digital-type input/output feeding sections) and its associated ideal building TFS (i.e., circuit scheme in Fig. 1 with $f_d = 2$ GHz, $Z_0 = 50$ Ω, $Z_1 = 98.3$ Ω, $Z_2 = 45.5$ Ω, $Z_3 = 64.7$ Ω, $Z_4 = 50.2$ Ω, $Z_5 = 119.4$ Ω, and $Z_L = 124.3$ Ω).

IV. Conclusion

A class of very-sharp-rejection broad-band BPFs shaped by two-stage-quadrature-coupler-based TFSs has been reported. It has been demonstrated that the employment of two-stage branch-line couplers loaded by shorter-length identical stubs in the building TFS—instead of one-stage couplers with longer dissimilar stubs—allows to augment the number of in-band reflection zeros and reduce the amplitude variation of its wide quasi-equiripple-type passband. Furthermore, inter-digital-type input/output feeding

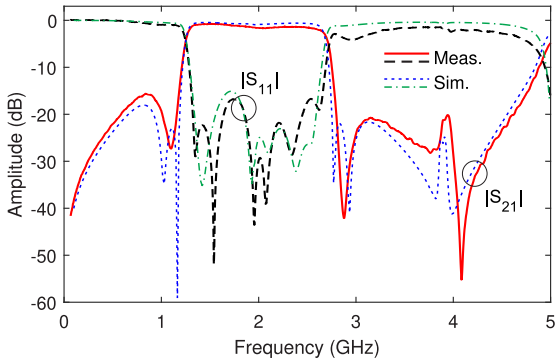

(a)

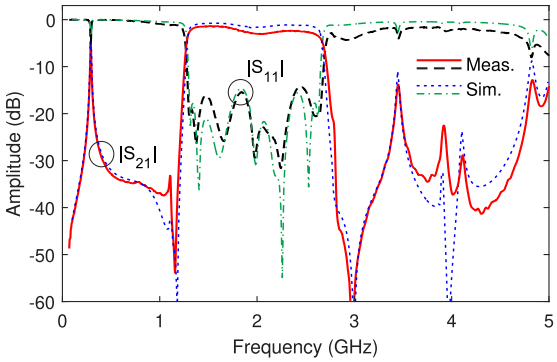

(b)

Fig. 9. EM-simulated and measured power transmission ($|S_{21}|$) and reflection ($|S_{11}|$) responses of the manufactured microstrip prototypes of wide-band BPFs. (a) Single-TFS circuit. (b) Two-TFS-based circuit.

cells can be inserted in the TFS to further increase the lower/upper stopband bandwidths and their rejection levels. The discrete-time modeling of this signal-interference BPF concept particularized in some illustrative examples towards its better understanding has also been provided. In addition, the experimental viability of wide-band BPFs based on this TFS approach has been verified through the design, EM-simulation, manufacturing, and testing of single- and two-TFS microstrip prototypes centered at 2 GHz.

ACKNOWLEDGMENT

This work has been supported in part by the Spanish Ministry of Science and Innovation (State Research Agency) under Project PID2020-116983RB-I00 and in part by the GOT ENERGY TALENT (GET) fellowship programme co-funded by the EU as part of the H2020-MSCA-COFUND programme (Grant Agreement number 754382).

REFERENCES

[1] C.-S. Lin, S.-F. Chang, and W.-W. Hsiao, "A full-360º reflection-type phase shifter with constant insertion loss," *IEEE Microw. Wireless Compon. Lett.*, vol. 18, no. 2, pp. 106–108, Feb. 2008.

[2] N. Youngthanisara, R. Phudpong, T. Rergmaneewan, and P. Booppha, "A novel 180º microstrip phase shifter based on cascaded branch-line couplers for direct QPSK modulation," in *Proc. 2010 Asia-Pacific Microw. Conf.*, Yokohama, Japan, Dec. 2010, pp. 488–491.

[3] W. Chen *et al.*, "Design and linearization of concurrent dual-band Doherty power amplifier with frequency-dependent power ranges," *IEEE Trans. Microw. Theory Techn.*, vol. 59, no. 10, pp. 2537–2546, Oct. 2011.

[4] J. Yao, C. Lee, and S.-P. Yeo, "Microstrip branch-line couplers for crossover application," *IEEE Trans. Microw. Theory Techn.*, vol. 59, no. 1, pp. 87–92, Jan. 2011.

[5] Q. Wu, A. Zhang, Y. Yang, M. Yu, and X. Shi, "Computed-aided tuning of Butler matrices," *IEEE Trans. Microw. Theory Techn.*, vol. 67, no. 11, pp. 4386–4393, Nov. 2019.

[6] R. Gómez-García, J.I. Alonso, and D. Amor-Martín, "Using the branch-line directional coupler in the design of microwave bandpass filters," *IEEE Trans. Microw. Theory Techn.*, vol. 53, no. 10, pp. 3221–3229, Oct. 2005.

[7] R. Gómez-García and M. Sánchez-Renedo, "Microwave dual-band bandpass planar filters based on generalized branch-line hybrids," *IEEE Trans. Microw. Theory Techn.*, vol. 58, no. 12, pp. 3760–3769, Dec. 2010.

[8] J.-M. Muñoz-Ferreras, D. Psychogiou, R. Gómez-García, and D. Peroulis, "A substrate-integrated-waveguide dual-band bandpass filter based on signal-interference principles," in *Proc. 2017 IEEE Radio Wireless Symp.*, Phoenix, AZ, USA, Jan. 15–18, 2017, pp. 125–127.

[9] A. C. Guyette, I. C. Hunter, and R. D. Pollard, "Design of absorptive microwave filters using allpass networks in a parallel-cascade configuration," in *Proc. IEEE MTT-S Int. Microw. Symp. Dig.*, Boston, MA, USA, Jun. 2009, pp. 733–736.

[10] M. Fan, K. Song, L. Yang, and R. Gómez-García, "Frequency-tunable constant-absolute-bandwidth single/dual-passband filters and diplexers with all-port-reflectionless behavior," *IEEE Trans. Microw. Theory Techn.*, vol. 69, no. 2, pp. 1365–1377, Feb. 2021.

[11] R. Gómez-García, "High-rejection wideband signal-interference microstrip filters using rat-race couplers," *IEE Electron. Lett.*, pp. 1162–1163, vol. 42, no. 20, Sept. 28th, 2006.

[12] M.-Á. Sánchez-Soriano, E. Bronchalo, and G. Torregrosa-Penalva, "Dual band bandpass filters based on strong coupling directional couplers," in *Proc. 39th Eur. Microw. Conf.*, Rome, Italy, Sep. 29–Oct. 1, 2009, pp. 1401–1404.

[13] R. Gómez-García and M. Sánchez-Renedo, "Application of generalized Bagley-polygon four-port power dividers to designing microwave dual-band bandpass planar filters," in *Proc. 2010 IEEE MTT-S Int. Microw. Symp.*, Anaheim, CA, USA, May 23–28, 2010, pp. 580–583.

[14] A. Morini *et al.*, "Systematic evaluation of spikes due to interference between cascaded filters," *IEEE Trans. Microw. Theory Techn.*, vol. 66, no. 11, pp. 4814–4819, Nov. 2018.

[15] J.-M. Muñoz-Ferreras and R. Gómez-García, "A digital interpretation of frequency-periodic signal-interference microwave passive filters," *IEEE Trans. Microw. Theory Techn.*, vol. 62, no. 11, pp. 2633–2640, Nov. 2014.

[16] J.-M. Muñoz-Ferreras, D. Psychogiou, and R. Gómez-García, "Digital modeling of microwave filters with coupled-line sections," in *Proc. 2019 IEEE MTT-S Int. Conf. Numer. Electromagn. Multiphys. Modeling Optim.*, Cambridge, MA, USA, May 29–31, 2019, pp. 1–4.

[17] S. Sun and L. Zhu, "Wideband microstrip ring resonator bandpass filters under multiple resonances," *IEEE Trans. Microw. Theory Techn.*, vol. 55, no. 10, pp. 2176–2182, Oct. 2007.

[18] S. Sun and L. Zhu, "A compact wideband bandpass filter using transversal resonator and assymmetrical interdigital coupled lines," *IEEE Microw. Wireless Compon. Lett.*, vol. 18, no. 3, pp. 173–175, Mar. 2008.